Walailak J Sci & Tech 2005; 2(2):135-148.

Flash Flooding Area Prediction by GOES-9 Satellite Data

Watcharee RUAIRUEN, Krisanadej JAROENSUTASINEE and Mullica JAROENSUTANEE

School of Science, Walailak University, Thasala, Nakhon Si Thammarat 80160, Thailand.

ABSTRACT

In this study, a new geocomputing index called the Rain Exposure Index (REI) is proposed. REI can be used for flash flooding prediction due to heavy rainfall accumulation. The index was constructed by computing data from GOES-9 satellite images using combinations of image processing and functional constructs. Water vapour data from GOES-9 satellites were collected from 1st January - 20th September, 2005. Thresholding techniques and varied thresholding values from 65-80 with 5 point intervals were used. REI forecasting results were compared with Thai Meteorological Department (TMD) results. The results indicated that 65-70 thresholding values provided a higher percentage of correct prediction than 75-80 thresholding values. Comparsion between the REI and TMD predictions, found that the REI gave a better correct warning of an event than TMD forecasting.

Key words: Geocomputing index - Flood risk area
Rain exposure index (REI) - Geostationary operational environmental satellites 9 (GOES-9) satellite

INTRODUCTION

Flood disasters are the most frequent and devastating natural disaster in South East Asia resulting in loss of life and wide spread damage to property. For the past 30 years, the number of flood disasters has increased compared to other forms of disaster (1). Increases in the frequency or intensity of extreme precipitation events exacerbate risks of disastrous flooding both in upland watersheds where such events can trigger landslides, and in lower floodplains which are often densely settled (2). Although there are many reasons for flooding, one of the principle reasons is climate (lose of more life and wide spread damage to property). The characteristics of flooding events in local Thailand have two forms, which are “flash flood” where the lag time between peak of rainfall intensity and flood event might be in a span of only few hours, and “river flood” where the lag time might be days, or weeks. Floods are now seen as a hazard that has to be controlled (3). However, the majority of countries do not document or map flooding scientifically (4).

Water remains stagnant after the flood recedes, sources of drinking water get polluted and food becomes spoiled (5). Inevitably, floods become a part of our living system and it is impossible to avoid them. It is then necessary to learn and understand the causes of flooding in order to reduce the damages and losses. Several approaches are used to lessen the destruction including forecasting the possibility of having flooding and identifying flood-prone areas.

In the last year, meteorological data such as rainfall estimation based on remote sensors in the visible (VIS), infrared (IR) radar, and microwave (MW) ranges of the spectrum, have been carried out on board several launched platforms. In particular, the launch of the newest generation of geostationary satellites, the Geostationary Operational Environmental Satellite GOES-I-M series (6) and the newest METEOSAT Second Generation (MSG) (7) with its Spinning Enhanced Visible and Infrared Imager (SEVIRI), adds new channels to the traditional VIS-IR-WV (Water vapour) triplet. One particular type of satellite data that this study is interested in is the GOES satellite imagery. They carry two separate radiometer packages which are an imager and a sounder. The imager has one water vapour channel (channel 3); while the sounder has three water vapour bands (bands 10,11,12). These channels/bands are sensitive to radiation at various wavelength intervals with in the 6.5 - 7.4 μm range. GOES-9 satellite circles the Earth in a geosynchronous orbit, which means that they orbit the equatorial plane of the Earth at a speed matching the Earth's rotation. They are designed to operate in the geosynchronous orbit 35,790 km above the Earth surface. They provide a constant vigil for the atmospheric triggers for severe weather conditions such as tornadoes, flash floods, hailstorms, and hurricanes. The satellites receive transmissions from free-floating balloons, buoys and remote automatic data collection stations around the world.

Water vapour absorbs and reradiates electromagnetic radiation in various wavelength bands. Such infrared radiation emitted by the Earth/atmosphere is intercepted by satellites. Water vapour molecules in the atmosphere absorb outgoing terrestrial radiation in the infrared region of the electromagnetic spectrum. The AVHRR sensor on the NOAA polar orbiting satellites has two thermal channels, near 11 and 12 μm, which are designed to correct for water vapour effects when predicting sea-surface temperatures (8)**.** Several investigators have employed these thermal channels in estimating total column water vapour (or PWV) from the AVHRR sensor (~1.1 km at nadir) in a technique referred to as the split-window technique (9,10,11). Water vapour data from GOES-9 satellite showed water vapour in the upper troposphere, the only area of the atmosphere generally important in everyday weather forecasting. These systems have a large effect on weather patterns found at the surface.

This study aimed at developing a new technique to predict the flood risk areas called the Rain Exposure Index (REI). REI was constructed using a combination of image processing and functional constructs using real-time water vapour data from GOES-9 satellites. REI was able to predict flood risk areas due to heavy rainfall, which is normally difficult to predict in time. Then we compared REI results with the Thai Meteorological Department (TMD) forecasting.

MATERIALS AND METHODS

Study Area

Study areas were located at latitude -5°S - 45°N and longitude 90°E - 150°E. We used 2-minute (1 minute of latitude = 1 nautical mile, or pproximately 1.852 km) resolution terrain and topography from ETOPO2 data (12) to generate coastal contour lines for South East Asia. In this study, we focused our work on the Thai boundary. Thailand covers an area of 513,115 km^2 between latitude 6°-21°N and longitude 98°-105°E.

GOES-9 Satellite Data

In this study, we used water vapour data from GOES-9 satellites. Water vapour images were one of a new series of advanced geostationary sensors with improved infrared spatial resolution and radiometric sensitivity (13). Water vapour images from the GOES-9 satellite were updated every 30-min at http://www.nrlmry.navy.mil/archdat/pacific/western/tropics/vapor/ (14) **(Figure 1)**. Multi-temporal datasets of GOES-9 satellite were used during 1st January - 20th September, 2005.

Rain-Gauge Data Collection

Rain-gauge data have been the main source of daily rainfall data (15). In this study, rain-gauge data during 1st January - 20th September, 2005 were obtained from the web site of the Royal Irrigation Department (16) and the Thai Meteorological Department. Flooding events usually occur when the amount of daily rainfall is over 40 mm/day (17,18). We selected 50 rain-gauge stations from the provinces where flooding and non-flooding events occurred such as Chiangmai, Chiangrai, Nan, Maehongson, and Nakhonsawan.

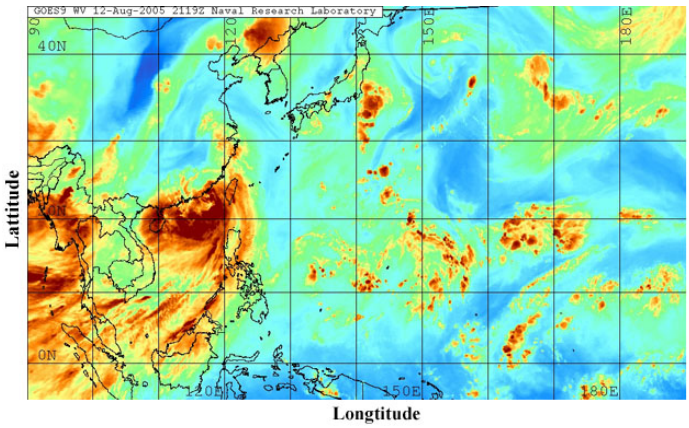

Figure 1. Water vapour data from GOES-9 satellite in South East Asia. This image was acquired on 12 August 2005. Dark areas represent high water vapour, which means heavily rainfall (14).

Digital Image Processing Technique

Water vapour data from GOES-9 were obtained from IR sensors, which gave the digitized value from 0 to 255. Water vapour data were then transformed to RGB colours by the Navy department, USA in JPEG format. We then downloaded the vapour maps from the navy website to our local archive automatically at half an hour intervals. These data allowed us to trace back water vapour information for any specific area in South East Asia. Each image was decomposed into three-single colour channels {i.e. red, green and blue (RGB)} (19). A hypothetical rain-indicating index was constructed by inverting the green channel and re-combining it with the red channel. The image was then changed into a grey level image ranging from 0 to 1, where 0 and 1 represented black and white, respectively. The grey level values of an RGB colour image, denoted $\overline{f}(x,y)$, were computed using *{r(x, y), g(x, y), b(x, y)}* in Eq. (1) (20). We converted RGB colours to a grey scale image by combining the red, green, and blue signals in proportion to the human eye's sensitivity to them. In this study, we chose the weighting coefficients shown in Eq. 1.

$$\overline{f}(x,y) = 0.299r(x,y) + 0.589g(x,y) + 0.114b(x,y) \quad [1]$$

Where, r = red, g = green, b = blue, x and y were spatial (plane) coordinates, and the amplitude of f at any pair of coordinates *(x, y)* was called the intensity or grey level of the image at that point. A monochrome digital image *f (x, y)* was a 2D array of luminance (brightness) values Eq. (2),

$$f(x,y) = \begin{pmatrix} f(0,0) & f(0,1) & \cdots & f(0,N-1) \\ f(1,0) & f(1,1). & & f(1,N-1) \\ \vdots & & \ddots & \vdots \\ f(M-1,0) & f(M-1,1) & \cdots & f(M-1,N-1) \end{pmatrix} \quad [2]$$

With $f(x,y) \in Z$, where Z was the domain of the integers, and $0 \le f(x,y) \le L-1$, where typically $L = 256$. Each element of the array was called a pel (i.e. picture element), or more commonly pixel. Values in this range can be efficiently represented by 8 binary digits (note that $2^8 = 256$) and therefore, each pixel occupied one byte in memory. Total storage requirements for an image were therefore of the order of M×N bytes, where M and N were the number of rows and columns in the image array, respectively.

Flash floods occur in short time scales over which flood producing rainfall occurs (generally < 6 hours) over small spatial scales. Therefore, 24 images (12 hrs) were used in the study. REI was constructed by integrating all 24 images using an image multiplication technique. If there were high amounts of water vapour in all 24 images, the REI would be high. This high REI means a high probability of heavy rainfall in 12 hrs (i.e. flash flooding). The final image was transformed to pixel with values ranging from 0-255. These images contained only two principal grey-level regions **(Figure 2a)**.

The next step of the algorithm was to threshold the final image in order to decide which pixels in the image corresponded to flood risk areas. A thresholding technique is a well-known technique for image segmentation (21,22). Grey-level images were converted into binary images (23). The final image was segmented into two classes using a global threshold **(Figure 2b)**. In the final binary image, each pixel value was determined or assigned to hold the values of 0 or 1 based on a comparison criteria with some global threshold value (*T)*, e.g. by Eq. (3).

$$f_T(x,y) = \begin{cases} 1, & if \quad f(x,y) \ge T \\ 0, & if \quad f(x,y) < T \end{cases} \quad [3]$$

Where, *x, y* = x, y coordinates and *T* = threshold value

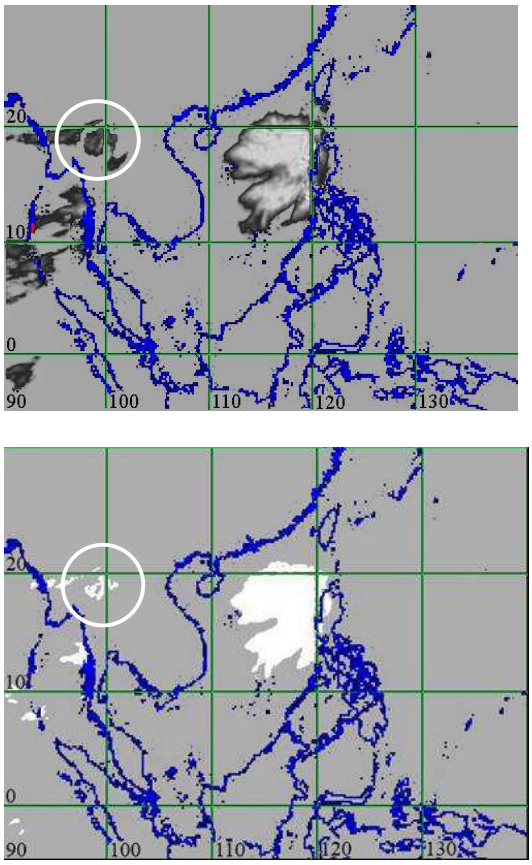

(a)

(b)

Figure 2. REI images for flash flooding in Chiangmai Province on 13th August 2005 (white circle), (a) before using a 70 thresholding value, and (b) after using a 70 thresholding value.

However, given some appropriate measurement of the quality of the segmentation, automatic threshold selection algorithms can be derived. The function [OptimumThreshold] returned a threshold value based on one of two user selectable minimisation criteria. The user may select a threshold value that minimised the mean squared error between the original and the binary image or one that minimised the weighted sum of group variances, where the group variances were formed from the pixels that fell above and below some chosen threshold (24). The function [OptimumThreshold] gave different threshold values for each flooding event. The images contained only two principal grey-level regions (25). Then, we viewed these values as random quantities, and plotted the histogram to estimate the probability density function (26). We used 87 reported non-flooding events and 13 reported flooding events to determine the thresholding value that gave the most correct predictions. We used the report of flooding and non-flooding events from TMD, newspapers, the Civil Defence Secretariat, the Royal Thai Police, and the Department

of Pollution Control report to obtain flooding events. We varied thresholding values from 0-255 values to determine which range of thresholding value that could detect flooding events. After we found that range, we tested the range in 5 value intervals in order to get a more precise thresholding value. The histogram was the probability density function of a random variable **(Figure 3)**. The final image with the flooding area should be shown in white colour called REI.

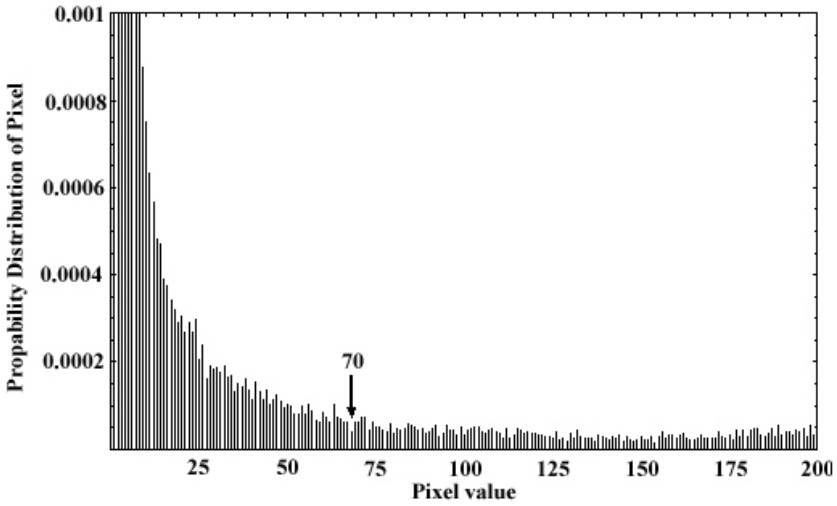

Figure 3. Histogram of the final image with an arrow pointing at the 70-thresholding values.

Forecasting and Validation of Flooding Area

This study forecasted flood risk areas during 1st August - 20th September, 2005 by using the REI forecasting model. We used the report of flood warning events from TMD. We checked for the flooding events from newspapers and the Civil Defence Secretariat, the Royal Thai Police, and the Department of Pollution Control report. We compared the REI forecasting results with the TMD forecasting results.

The validation step was performed using the amount of daily rainfall data from the Royal Irrigation Department, Thailand at Chiangmai, Maehongson, and Nakhonsawan provinces. We plotted the amount of daily rainfall through time and expected a high amount of daily rainfall during flooding events by using *Mathematica*. Then, we compared the amount of daily rainfall to see if a high amount of daily rainfall occurred at the same period as when the REI and TMD predicted flooding events. If there were some events that were predicted by the REI forecasting as flooding events but these flooding events were not reported by the TMD as flooding events, then we plotted an amount of daily rainfall to see if the amount of daily rainfall was more than 40 mm/day. If so, this suggested that it would be very likely that a flooding event would occur. We would use a high amount of daily rainfall as an indicator of flooding events. Therefore, the amount of daily rainfall was plotted during the time that the REI predicted flooding.

Data Analysis

Chi-Square tests were used to test whether the REI and TMD made a correct prediction greater than 50% of the time. A Chi-Square test was also used to compare whether the REI and TMD gave the same correct prediction.

RESULTS AND DISCUSSION

After using an image processing technique at the 70-thresholding value, the final image showed flooding risk areas, indicated in white colour **(Figure 4)**. We used 87 reported non-flooding events and 13 reported flooding events to determine the thresholding value that gave the most correct predictions. We found that 65-80 thresholding values could be used to predict the flood risk area. When thresholding values were varied from 65-80 with 5-value intervals, 65 and 70-thresholding values gave a more accurate prediction than 75 and 80-thresholding values **(Table 1, Figure 4a-d)**. Therefore, 65-70-thresholding values should be used in the REI because these thresholding values gave a better prediction of flood risk area.

TMD showed 50% false predictions on flooding/non-flooding events **(Table 2)**. On the other hand, REI correctly predicted flooding/non-flooding events greater than 50% probability. When we compared between the REI and TMD predictions, we found that the REI gave a better correct warning event than TMD forecasting {Pearson Chi-square test: $\chi^2_{1st} = 9.36$, $P < 0.05$ **(Table 2)**}.

During 1st - 31st August 2005, there were two reported flooding events from both TMD and REI forecasting. The amount of daily rainfall during these two flooding events was higher than non-flooding events **(Figure 5)**. However, there was one event that was predicted by the REI forecasting as a flooding event but was not reported by the TMD as a flooding event (i.e. during 20th - 23rd August, 2005) **(Figure 5)**. If we consider the amount of daily rainfall, this event should result in flooding as REI predicted because the amount of daily rainfall during that period was much higher than 40 mm/day.

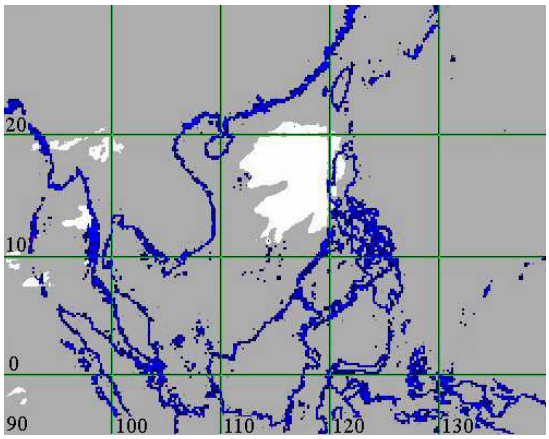
20
10
0
90
100
110
120
130

(a)

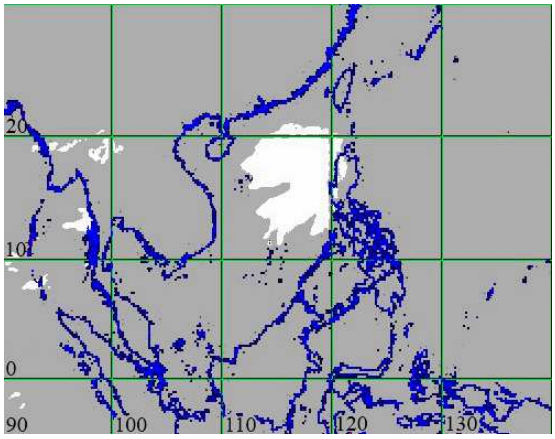
20
10
0
90
100
110
120
130

(b)

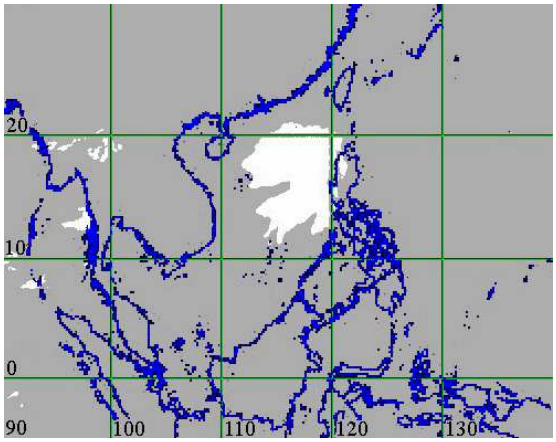
20
10
0
90
100
110
120
130

(c)

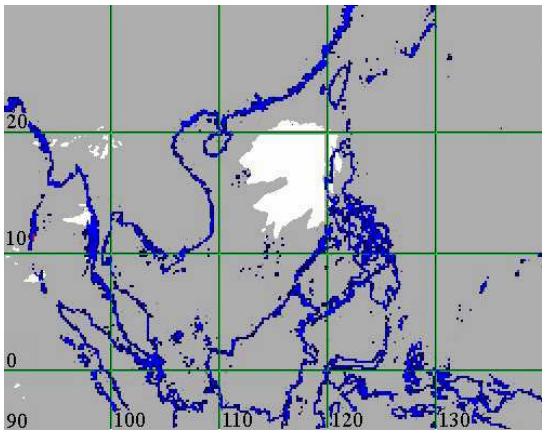

(d)

Figure 4. REI images for flash flooding with 65-80-thresholding values: (a) 65, (b) 70, (c) 75 and (d) 80.

There are few spatial and temporal data available on flooding events and even fewer models that provide accurate flooding predictions in time. Besides TMD forecasting, REI forecasting offers a new way to predict flooding events. In short, REI could help in preventing serious damage and may help to decrease the death and economic disaster from serious flooding.

However, there were limitations of the current technique. This technique depends on the real time availability of the data from GOES-9 satellites. They would have a problem with our technique if water vapour data that were collected were not complete. Another limitation is the resolution of the on-board satellite sensors. For current GOES-9 satellites the resolution is somewhat at mesoscale, so it is not possible to pinpoint a small size location such as Tambon or district. Besides, using the acquisition of hydrological data including variables relating to flow velocities, erosion, sedimentation, discharge patterns topography/terrain data were needed. Finally, at the time of doing this research, we have very limited access to data from some departments to validate our technique.

Table 1. Accuracy assessment of four thresholding values. *n* represents the number of events.

Thresholding Value	Non-flooding Events		Flooding Events	
	(*n* = 87)	Accuracy (%)	(*n* = 13)	Accuracy (%)
65	87	100	12	92.31
70	87	100	12	92.31
75	87	100	11	84.62
80	87	100	11	84.62

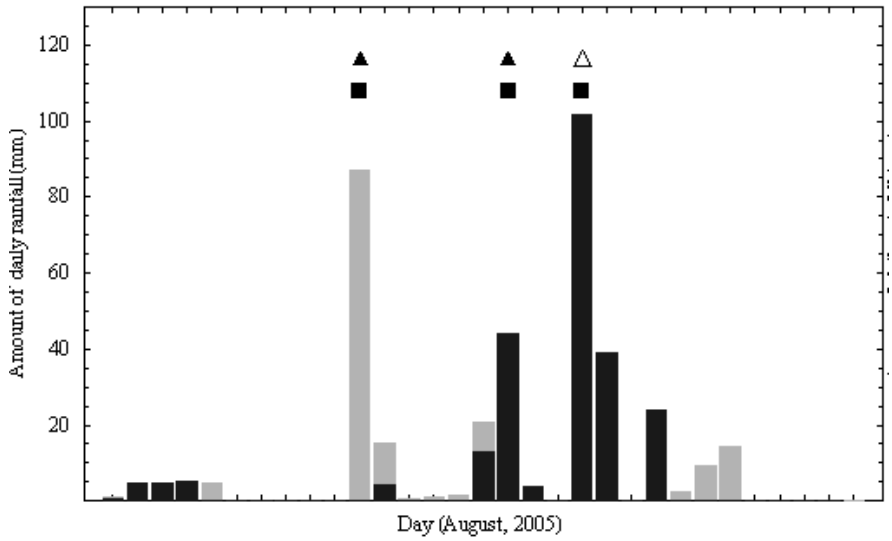

Figure 5. The amount of daily rainfall (mm) from rain-gauge stations in (■) Chiangmai and (■) Nakhonsawan Provinces. Closed and open symbols represent flooding and non-flooding predictions, respectively; □, Δ represent REI and TMD forecasting, respectively.

Table 2. The accuracy of warning events between TMD and REI forecasting techniques. *$P < 0.01$

Forecasting Technique	Correct Warning Events	False Warning Events	Statistic test
TMD	13	8	$\chi_1^2 = 1.19$
REI	15	3	$\chi_1^2 = 8.00$ *
Total	**28**	**11**	

ACKNOWLEDGEMENTS

We thank Asst. Prof. Dr. David Harding and Robert J. Santos for comments on the previous versions of this manuscript. We also thank the Thai Meteorological Department and the Royal Irrigation Department for providing weather data. This project was supported by CX-KURUE and the Institute of Research and Development, Walailak University.

REFERENCES

1) Dutta D Herath S. Trend of floods in Asia and flood risk management with integrated river basin approach. 1st Asia-Oceania Geosciences Society Annual Meeting, July 4th - 9th, 2004.
2) Kundzewicz ZW Schellnhuber HJ. Floods in the IPCC TAR perspective. *Nat Hazards 2004; 31: 111-28.*
3) Manuta J Lebel L. Climate change and the risks of flood disasters in Asia: Crafting adaptive and just institutions. *Human Security and Climate Change*, An International Workshop Holmen Fjord Hotel, Asker, near Oslo; June 21st - 23rd 2005.
4) Choudhury NY Paul A Paul BK. Impact of coastal embankment on the flash flood in Bangladesh: a case study. *Appl Geogr 2004; 24: 241-58.*
5) O'Donnell S. Weather radar enhanced flash flood forecasting. *Proceedings of Open source GIS - GRASS users conference Trento Italy; September 11st - 13rd, 2002.*
6) Menzel WP Purdom JFW. Introducing GOES-I: The First of a New Generation of Geostationary Operation Environmental Satellites. *B Am Meteorol Soc 1994; 75: 757-82.*
7) Schmetz J Pili P Tjemkes S Just D Kerkmann J Rota S Ratier A. An Introduction to Meteosat Second Generation (MSG). *B Am Meteorol Soc 2002; 83: 977-92.*
8) Mcmillan LM Crosby DS. Theory and validation of the multiple window sea surface temperature. *J Geophy Res 1984; 89: 3655-61.*
9) Dalu G. Satellite remote sensing of atmospheric water vapour. *In J Res 1986; 7: 1089-97.*
10) Kleespies TJ Mcmillin LM. Retrieval of precipitable water from observations in the split window over varying surface temperatures. *J Appl Meteor 1990; 29: 851-62.*
11) Roger JC Vermote EF. A method to retrieve the reflectivity signature at 3.75 µm from AVHRR data. *Remote Sensing of the Environment 1998; 64: 103-14.*
12) ETOPO2 data [On-line]. Available from: www.ngdc.noaa.gov/mgg/image/2minrelief.html. 10 October 2005.
13) Ellrod GP Achutuni RV Daniels JM Prins EM Nelson JP III. An assessment of GOES-8 imager data quality. *B Am Meteorol Soc 1998; 79: 2509-26.*
14) Water vapour data from GOES-9 satellite [On-line]. Available from: http://www.nrlmry.navy.mil/archdat/ pacific/western/tropics/vapor/10 October 2005.
15) Grimes DIF Prado-Igu′zquiza E Bonifacio R. Optimal a real rainfall estimation using rain guages and satellite data. *J Hydrol 1999; 222: 93-108.*
16) Rainfall data [On-line]. Available from: http://www.kromchol.com/hydroweb/UpdateDR.asp. 10 October 2005.
17) Karl TR Knight RW Plummer N. Trends in high frequency climate variability in the twentieth century. *Nature 1995; 377: 217-20.*
18) Yu B Neil DT. Long-term variation in regional rainfall in the south-west of western Australia and the difference between average and high intensity rainfalls. *Int J Climatol 1993; 13: 77-88.*
19) Image Processing Toolkit 1992; 1 [On-line]. Available from: http://www.wolfram.com/. 10 October 2005.
20) Wolfram S. The *Mathematica* Book, Fifth Edition, Book News, Oregon, 2004.

21) Haralick RM Shapiro LG. Computer and Robot. Vision Addison-Wesley Reading MA 1992.
22) Sahoo PK Soltani S Wong AKC. A survey of thresholding techniques. *Comput Vis Grap Image Proc 1988; 41: 233-60.*
23) Tizhoosh HR. Image thresholding using type II fuzzy sets. *Pattern Recogn 2005; 38: 2363–72.*
24) Otsu N. A threshold selection method from gray-level histograms. *IEEE Trans Syst Man Cybern 1979,* SMC-9.
25) Gonzalez RC Woods RE. Image Segmentation. *In*: Digital Image Processing: Second Edition. Pearson Education (Singapore) Pte. Ltd., Indian Branch, 2002; p. 567-636.
26) Wickham-Jones T. *Mathematica* Graphics Techniques and Application. Wolfram Research, Inc., 1994: p. 54-77.

บทคัดย่อ

วัชรี รวยรื่น กฤษณะเดช เจริญสุธาสินี และ มัลลิกา เจริญสุธาสินี

การทำนายพื้นที่การเกิดน้ำท่วมฉับพลันด้วยภาพถ่ายดาวเทียม GOES-9

การศึกษานี้ได้เสนอดัชนีค่า Rain Exposure Index (REI) ซึ่งสามารถใช้ทำนายน้ำท่วมฉับพลันอันเนื่องมาจากการเกิดฝนตกหนัก ดัชนีนี้ถูกสร้างและคำนวณมาจากข้อมูลภาพถ่ายดาวเทียม GOES-9 โดยใช้การรวมกันของการวิเคราะห์ภาพและสร้างฟังก์ชัน ข้อมูลภาพถ่ายปริมาณไอน้ำจากดาวเทียม GOES-9 ที่ใช้ในการศึกษาอยู่ระหว่างวันที่ 1 สิงหาคม จนถึงวันที่ 20 กันยายน 2548 ในการศึกษาได้ใช้ค่า Threshold 4 ค่าซึ่งอยู่ในช่วงตั้งแต่ 65-80 ผลจากการทำนายด้วย REI ได้ถูกนำไปเปรียบเทียบกับผลการทำนายของกรมอุตุนิยมวิทยา (TMD) ผลจากการศึกษาพบว่าค่า Threshold ในช่วง 65-70 ให้เปอร์เซ็นต์ความถูกต้องสูงกว่าค่า Threshold ในช่วง 75-80 REI สามารถทำนายน้ำท่วมฉับพลันได้ถูกต้องมากกว่าการทำนายของ TMD

สำนักวิชาวิทยาศาสตร์ มหาวิทยาลัยวลัยลักษณ์ อำเภอท่าศาลา จังหวัดนครศรีธรรมราช 80160